Journal of Alloys and Compounds 505 (2010) 645–653

Contents lists available at ScienceDirect

Journal of Alloys and Compounds

journal homepage: www.elsevier.com/locate/jallcom

Microstructure and interfacial evaluation of Co-based alloy coating on copper by pulsed Nd:YAG multilayer laser cladding

Hua Yan [a], Aihua Wang [a,*], Kaidong Xu [a], Wenyan Wang [b], Zaowen Huang [a]

[a] State Key Laboratory of Materials Processing and Die & Mould Technology, Huazhong University of Science and Technology, Wuhan 430074, PR China
[b] School of Materials Science and Engineering, Henan University of Science and Technology, Luoyang 471003, PR China

ARTICLE INFO

Article history:
Received 7 April 2010
Received in revised form 12 June 2010
Accepted 15 June 2010
Available online 25 June 2010

Keywords:
Laser cladding
Co-based alloy
Multilayer
Interface
Microstructures

ABSTRACT

Laser cladding defect-free coatings on copper is rather difficult. The purpose of this study is to fabricate high quality Co-based alloy coating on copper substrate by laser cladding. Powder preplacement with a thickness of 0.7 mm improves the absorptivity of copper substrate to laser effectively and generates defect-free coating. Microstructures, phase constitutions and wear properties are investigated by means of scanning electronic microscopy (SEM) with X-ray energy dispersive microanalysis (EDX), transmission electron microscopy (TEM) and X-ray diffraction (XRD), as well as dry sliding wear test. Experimental results show that α-Co solution, $Cr_{23}C_6$, $Ni_{17}W_3$ and $Cr_4Ni_{15}W$ are the main phases in the Co-based coating. The Ni-based solid solutions (α-Co, Ni) and (Ni, Cu) are formed at interface, which generate metallurgical bonding by diffusion between Co-based coating and copper substrate. The average microhardness of the coating is $478HV_{0.1}$. Wear resistance of copper is significantly improved by laser cladding Co-based alloy multilayer coating.

1. Introduction

The excellent thermal conductivity, outstanding electric capability, good elasticity of copper and its alloys make them interesting materials for applications involving electrical apparatus, machinery, metallurgical equipment and aerospace components, etc. However, due to the poor wear resistance, oxidation resistance and electric erosive resistance, the service life of copper components is decreased seriously in extreme conditions. Surface modification of copper is necessary without affecting or altering the properties of bulk components. For example, to expand the serviceability limitation of copper, electroplating [1], thermal spraying [2,3] and casting infiltration [4] have been adopted. However, the bonding strength between coatings and copper substrate is a critical problem using those methods. This problem can be overcome by laser surface cladding (LSC). LSC offers several advantages over other surface modification techniques. The most important one arises from the fact that LSC is a nonequilibrium method involving high cooling rates (10^3–10^8 K s^{-1}) which produce metastable phases by exceeding the solid-solubility limit beyond the equilibrium phase diagram with an excellent metallurgical bond to the substrate. Therefore, LSC has become an alternative technique to conventional methods in order to produce large area coatings over metallic substrates.

Relating literatures illustrate that LSC has made a considerable progress in the aspects of equipment, defects prevention and new coating materials over the past two years. For instance, based on the use of a single mode fibre laser and a powder mircrofeeder, a new process has been used to undertake micro-cladding to produce Co-based alloy on stainless steel strips with geometrical characteristics in the micrometer rang (width: 45 μm, height: 15 μm) [5]. In addition, a systematic comparison between the performance of a Yb:YAG monomode fibre laser and a Nd:YAG laser in the side LSC has been developed by del Val et al. [6] and the results indicated that fibre laser is only useful for very narrow coatings required while Nd:YAG laser is suitable for large area coatings. Furthermore, in cracking prevention respect, laser-induction hybrid cladding by powder feeding is effective to prevent from cracking in Ni-based coating [7]. Moreover, Wang et al. has added an austenitic stainless steel net in the Ni-, Co- and Fe-based alloy coatings to control the cracks during LSC and the crack density is significantly reduced [8]. What's more, researches on new coating materials have been carried out widely. For example, utilizing fibre laser with high scanning speeds, defect-free Ti45Nb coatings with excellent hardness (up to 1000 $HV_{0.05}$) on a mild steel substrate have been deposited by pre-placed powder LSC by Fallah et al. [9]. Zheng et al. [10] has designed and fabricated calcium phosphate bioceramic coating on titanium alloy (Ti–6Al–4V) by LSC and investigated the bioactivity of the coating in vitro via soaking in a simulated body fluid (SBF). In general, LSC shows great potential in coatings preparation.

Though LSC can be easily achieved for many nonferrous metals such as magnesium alloy [11], titanium alloy [10,12] and Ni-based

* Corresponding author. Tel.: +86 27 87540049; fax: +86 27 87540049.
E-mail address: ahwang@mail.hust.edu.cn (A. Wang).

0925-8388/$ – see front matter © 2010 Elsevier B.V. All rights reserved.
doi:10.1016/j.jallcom.2010.06.099

Table 1
LSC technological parameters used in the experiment.

Track	Laser power (W)	Scanning velocity (mm s^{-1})	Thickness of powder preplacement (mm)	Side shielding gas flow rate (l min^{-1})	Central shielding gas flow rate (l min^{-1})	Laser pulse duration (ms)	Laser frequency (Hz)
1	300	5	0.3	25	20	1.1	60
2	330	5	0.5	25	20	1.1	60
3	360	5	0.5	25	20	1.1	60
4	390	5	0.7	25	20	1.1	60
5	360	7	0.5	25	20	1.1	60
6	360	9	0.5	25	20	1.1	60
7	360	11	0.5	25	20	1.1	60

superalloy [13], it is difficult to prepare crack-free and nonporous coatings on copper, due to the good thermal conductivity, poor wettability with many other materials and reflectivity to laser beam during laser processing [14]. Recently, Crack-free Ni–Co duplex coating has been successfully cladded on copper substrate by continuous wave CO_2 laser by Liu et al. [15]. In their study, nickel-based powder with 20 wt% Cu was pre-deposited on the surface of copper substrate by plasma spraying, before Co-based alloy laser cladding, the sprayed coating was pre-heated. The wear properties of Ni–Co duplex coating were higher than copper substrate. In the same way of preheating copper substrate to 300 °C before cladding, Zhang et al. [16] have prepared Ni-based alloy coating onto pure copper. However, the method of pre-spraying or preheating the substrate has several obvious drawbacks such as the heat damage of the important components, low cladding efficiency, worsening the work conditions and high production cost [7].

Generally, direct LSC large-area high quality Co-based alloy coatings with adequate thickness onto copper has not been developed so far, neither the evaluation of interface between coatings and substrate. Moreover, LSC energy is directly affected by the interface interaction [17]. In this study, Co-based alloy multilayer coatings were fabricated onto copper by direct LSC using a pulsed Nd:YAG laser. The microstructure and interfacial evaluation were focused on. The purpose was to obtain wear-resistant coating with metallurgical bonding onto copper. Potential applications can be found as chill mould for continuous casting and electrical contacts.

2. Experimental procedures

In LSC experiments, the pulsed Nd:YAG laser had a maximum output power of 400 W and it was equipped with a computer controlled multiaxis positioning system and worktable. A rectangular pulse was adopted to obtain stable pulse-shape. The laser beam was focused by a focus lens with a focal length of 100 mm. The spot size of laser beam was approximately 1.5 mm on copper surface. Though powder injection is commonly employed in LSC, it was not selected in this study due to the high reflectivity of Cu to laser. As Ng et al. [14] produced molybdenum layer on copper by LSC in his work, uniformly powder beds were applied to increase the laser energy absorptivity of Cu surface.

The substrates of test coupon (40 mm × 30 mm × 10 mm) used for LSC were a copper alloy cut from continuous casting mould, with a composition of Cu–0.9Cr–0.26Zr (wt.%). The substrates were surface machined and sand blasted to remove surface oxide before cladding. The powder adopted was gas atomized spherical Co-based alloy powder with a nominated composition (wt.%) of C: 1.0–1.3, Cr: 17–21, Ni: 15–18, W: 7.0–8.0, Si: 0.2–0.4, Mn: ≤0.3, Fe: ≤1.0 and Co in balance. The size of the powder was in the range of 45–100 μm. The morphology of as-received powder is shown in Fig. 1. The powder was mixed with 5 wt.% acetyl-cellulose alcohol and pasted onto substrate and then dried by a furnace for 2 h. The thickness of the paste was controlled in the range of 0.3–0.7 mm. The laser-generated pool was protected using a nozzle [18] to ensure that LSC was carried out under a circumstance of nearly pure shielding gas. After each powder bed was cladded, the surface was cleaned to remove the remainders. The following powder paste was coated onto previous laser-clad layer. The multilayer coating was achieved by repeating 4 times. The thickness of the LSC coatings was measured with a vernier caliper.

In order to get relatively high quality coatings, the influences of LSC parameters such as laser pulse width, laser power, scanning speed and thickness of powder bed were investigated. The criteria are that a crack-free and dense coating with relatively smooth surface should be obtained. First, the surface of cladding tracks was examined by a stereology microscopy. Afterward, the cross-sections of the samples were prepared for measuring width and height of tracks. The parameters of track with higher deposition rate, defect-free and good aspect ratio (more than 3) were chosen for large-area cladding with an overlapping ratio of 40%.

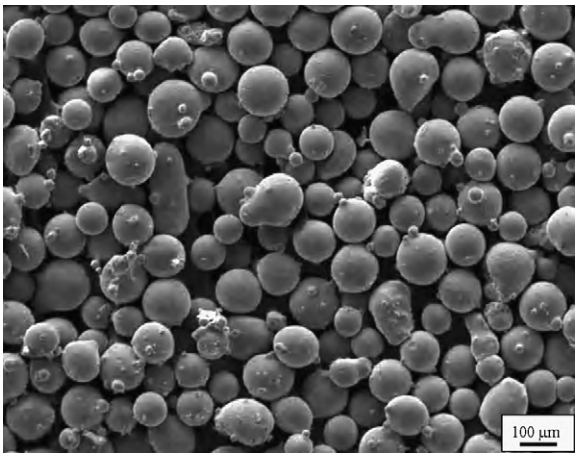

Fig. 1. Morphology of as-received Co-based alloy powder.

The cross-sections of the samples were prepared for microstructures analyses. The microstructures of the coatings were assessed using JSM-5610LV scanning electron microscope (SEM) with X-ray energy dispersive microanalysis (EDX). X-ray diffraction (XRD) test (Cu Kα, 1.54 Å wavelength radiation) was employed to determine the phases of the coating and interface by an X' Pert PRO X-ray Generator machine. A quick scan of 8° min^{-1} was primarily performed over a wide range of 2θ of 20–80°. A slower scan rate of 4° min^{-1} was further used over the 2θ range 42–45°, 50–52° to offer a more accurate determination of diffraction peaks [19]. FEI Tecnai G^2 20 transmission electron microscope (TEM) with EDX operating at 200 kV was used to investigate the microstructures. A microhardness measurement across the coating was carried out using a Buchler-3 microhardness tester with an applied load of 100 g for 15 s. Wear resistance of LSC coating and copper was evaluated by a pin-on-disc friction apparatus (MMS-1G) [20]. The material of disc was GCr15 steel and its hardness is HRC 60-62. The dimension of the disc was Ø 160 mm × 15 mm. The pin specimens with a dimension of Ø 14 mm × 40 mm were fixed. The wear test was performed by using sliding speed 2 m s^{-1} at a constant normal load 100 N under dry wear condition. The weight loss of wear specimens was quantified by an electronic balance with a minimum scale value of 0.1 mg.

3. Results

3.1. The effect of LSC parameters on surface morphology

In order to optimize the parameters for large-area cladding Co-based coating on copper, firstly, different laser pulse width (such as 0.5 ms, 1.0 ms, 1.5 ms and 2.0 ms) was used empirically with a fixed pulse frequency of 60 Hz. The beading-like and coarse surfaces of tracks were obtained when the laser pulse width was less than 1.0 ms with varying laser power from a lower value to a higher one at fixed scanning speed (5 mm s^{-1}). Low laser energy density and poor absorptivity of the laser in infrared area of Co-based alloy powder resulted in incomplete melting of the powder. When the laser pulse width was increased to 1.5 ms and 2.0 ms, the surfaces did not exhibit good aspect, either. After several trails, the laser pulse width and frequency were fixed at 1.1 ms and 60 Hz, respectively. After that, different laser processing parameters such as laser power, scanning speed and thickness of powder layer were studied.

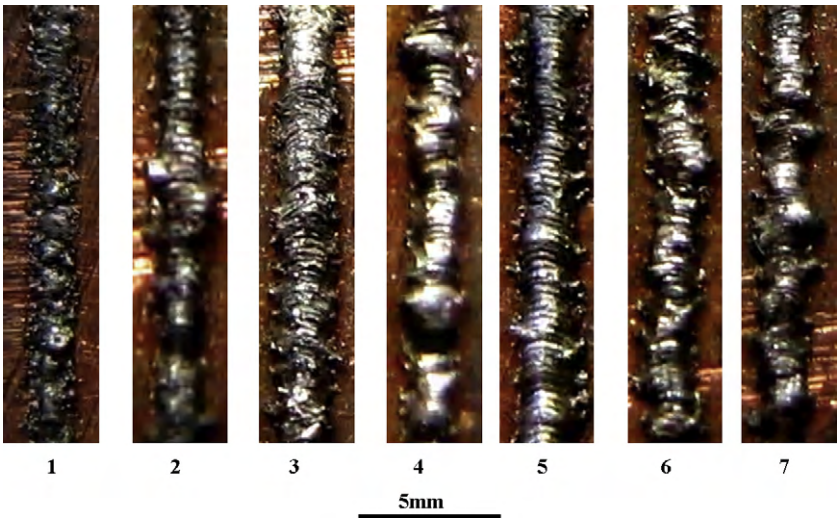

Fig. 2. Macroscopic of tracks with different process parameters.

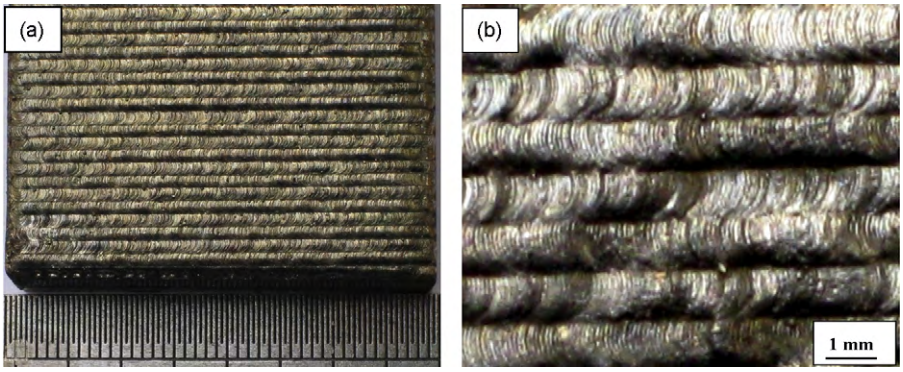

Fig. 3. Macroscopic morphology showing the surface of overlapping LSC multilayer coating.

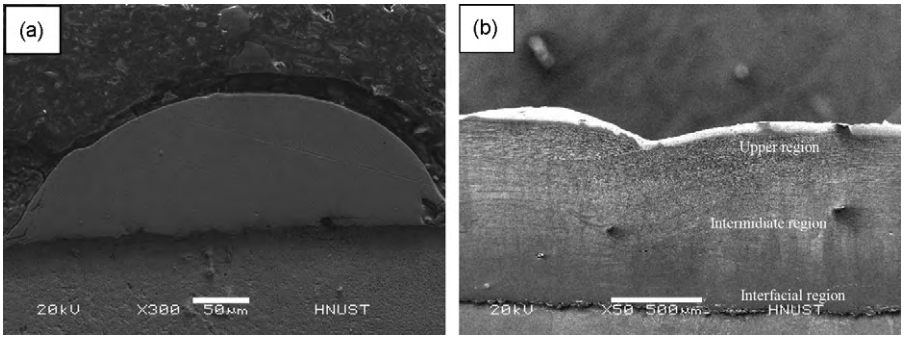

Fig. 4. Cross-section morphology of LSC Co-based alloy coatings on copper: (a) track 3 and (b) overlapping multilayer.

The surface features of tracks in different technical condition such as laser power, scanning speed and thickness of powder bed were observed. Macroscopic surface of the tracks is shown in Fig. 2 with the corresponding parameters tabulated in Table 1. It indicates that the deposition rate is low with thinner powder layer (0.3 mm). The defects such as welding beadings were formed (as track 1 shown in Fig. 2). The powder thickness was increased to 0.5 mm and the laser power energy was raised to 330 W and 360 W, respectively, the deposition rate was obviously increased (see track 2 and 3 in Fig. 2). However, when powder thickness and laser energy were increased, welding beadings were observed (as track 3 and 4 illustrated in Fig. 2). When scanning speed was increased 5 mm s^{-1} to 11 mm s^{-1} with a fixed laser energy power (360 W) and powder layer thickness (0.5 mm), the aspect ratio become smaller. In general, appropriate thickness of powder layer, reasonable laser power and scanning speed are required. Based on the results, since track 3 possessed the best aspect ratio and deposition rate, its parameters were chosen for overlapping cladding. Fig. 3 is macroscopic image of multitrack overlapping LSC multilayer coatings with the optimum parameters. Crack-free and nonporous surface can be obtained by LSC.

3.2. Microstructure and phase

Fig. 4 displays the SEM photographs of cross-section of track 3 and overlapping multilayer coating using secondary electron

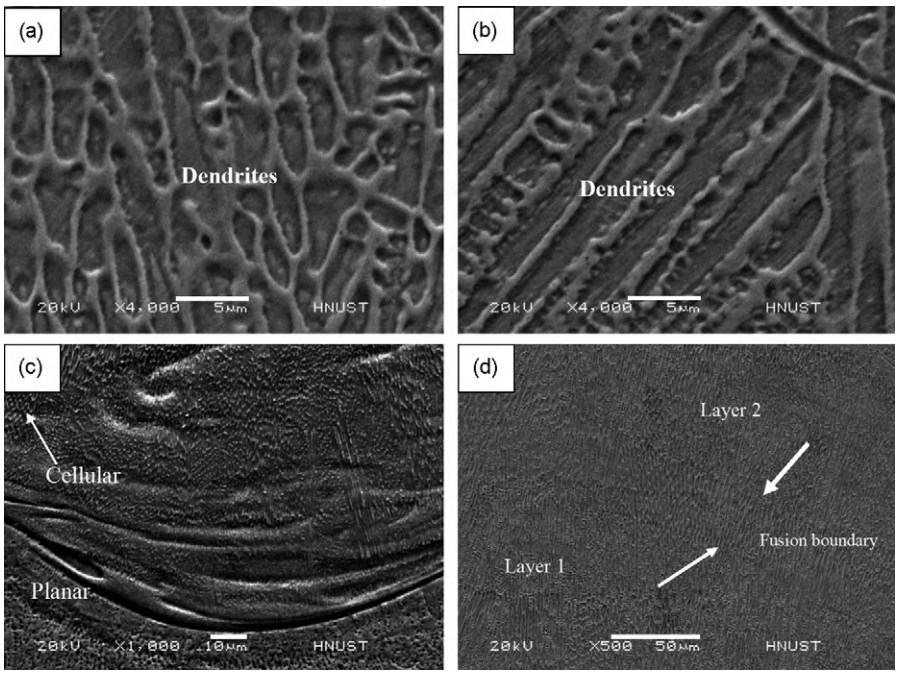

Fig. 5. Typical microstructures at different regions of LSC Co-based coating: (a) upper region; (b) middle region; (c) interface region and (d) Co/Co layers fusion region.

image. It is obvious that the coatings are crack-free and have a high-density. The height and width of the track is about 0.15 mm and 0.5 mm respectively, with an aspect ratio about 3. The overlapping multilayer coating with a total thickness about 1.5 mm was measured with a vernier caliper. The coatings/substrate interface had a smooth profile without cracks or pores (as shown in Fig. 4).

Typical microstructures of the multilayer sample at different locations (such as upper, middle and interfacial region) are shown in Fig. 5. The microstructures of the coating were mainly composed of dendrites in upper and middle regions (Fig. 5a and b), cellular and planar in bottom of molten pool (Fig. 5c). The clear and defect-free interface between the coating and substrate was observed, and well metallurgical bonding with 15 μm-thick layer was obtained at the bottom of the molten pool (Fig. 5c). It was distinctly seen that interfaces between Cu/Co and Co/Co layers were not flat or straight but of overlapped concave profile (as illustrated in Fig. 5c and d) due to the near Gaussian energy distribution of the laser beam. This waveform shape interface brings about the inconsistent depth of cladding coatings, but this would not significantly affect the main surface properties as long as the clad layer is homogeneous [14]. As well, the finer and more homogeneous microstructure was formed at the bottom of coating (Fig. 5c).

Fig. 6 depicts the XRD spectra of the LSC coating, which reveals the existence of α-Co solution (JCPDS index 89-4307), $Cr_{23}C_6$ (JCPDS index 85-1281), $Ni_{17}W_3$ (JCPDS index 65-4828) and $Cr_4Ni_{15}W$ (JCPDS index 65-5108). There are always different phases corresponding to one certain diffraction peak. Therefore, a step-scan method at a slower scan speed ($4^\circ\,min^{-1}$) was adopted for collecting X-ray diffraction data in the vicinity of 42–45°, and 50–52°. The phases were clearly revealed in Fig. 6(b) and (c). In general, the strong diffraction peaks corresponding to α-Co were clearly detected. Carbide and other intermetallics which contain element W were formed. However, the diffraction peaks of α-Co solution were moved somewhat toward left a small angle due to the solution of Cr, W and Si, etc. A similar result has been presented by Zhang et al. [16] LSC Ni-based alloy on copper using a CW CO_2 laser.

The diffraction peaks of phases in the interface/substrate region are further illustrated in Fig. 7. The sample for XRD had been ground down until the surface consisting mainly of a layer with small contributions of the coating. The XRD patterns of the interfacial region revealed existence of (α-Co, Ni) (JCPDS index 89-4307), (Ni, Cu) (JCPDS index 65-7246) solid solution and Cu (JCPDS index 70-3038). The Ni in as-received powder and Cu of substrate together formed the (Ni, Cu) solid solution by LSC. Different results were shown from the work by Dehm and Bamberger [21] LSC Co-based hardfacing on Cu using CO_2 laser. In his research, a large number of brittle phases were formed at the interface between the cladding and remelted plasma-sprayed layer, which can induce in cracks easily.

Fig. 8 depicts SEM morphology and EDX spectra of LSC coating. It could be seen that highly continuous dendrites were formed. To check the elementary composition of the different microstructures, EDX analyses were conducted, as shown in Fig. 8(b)–(d) and corresponding results were listed in Table 2. It was obvious that different atomic compositions existed as indicated by joint spider A and B. The EDX results revealed that such dendrites were $Cr_{23}C_6$ and α-Co which was rich in Cr and Co, while the interdendritic area was identified to be α-Co solid solution rich in Co. The rectangle C was in the fusion zone of two Co-based layers. The region between the two fusion boundaries was dense. The elemental contents in this area were between that of spot A and B, which represented the mean elemental distribution (see Table 2).

Fig. 9 shows the linear SEM-EDX across the interface between the coating and the copper substrate. It could be seen that a transition zone existed in interface region. The thickness of the transition zone was about 15 μm, as shown between the two white lines in Fig. 9(c). The content profile of Ni fluctuated slightly in the transition zone.

Table 2
Elemental atomic concentration for microstructures indicated in Fig. 8 by EDX analyses.

Spectrum	Chemical composition (at.%)				
	C	Cr	Co	Ni	W
A	47.50	18.99	27.16	4.81	1.54
B	12.43	26.24	48.83	10.35	2.15
C	33.62	19.04	38.85	7.29	1.20

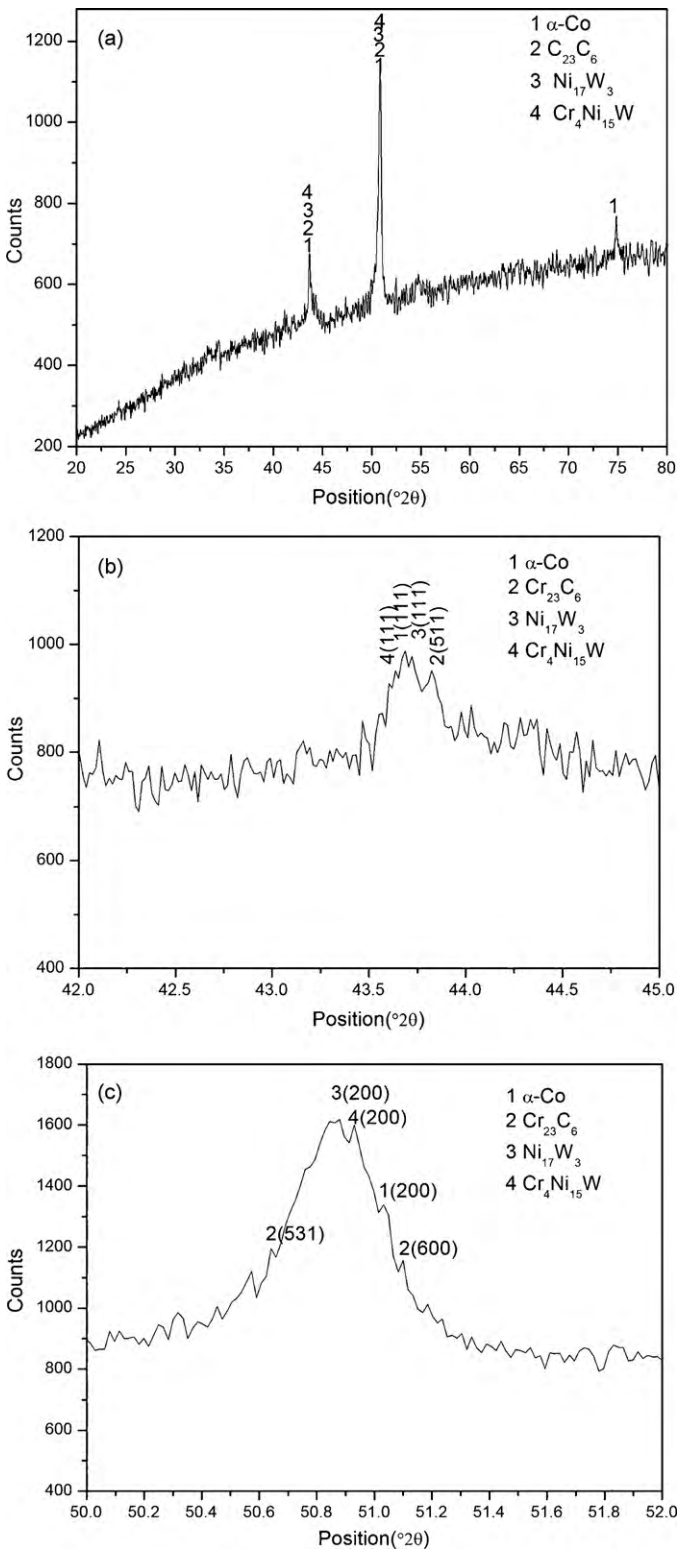

Fig. 6. XRD spectra of LSC Co-based alloy coating: (a) 20–80°, (b) 42–45° showing the details, and (c) 50–52° for details.

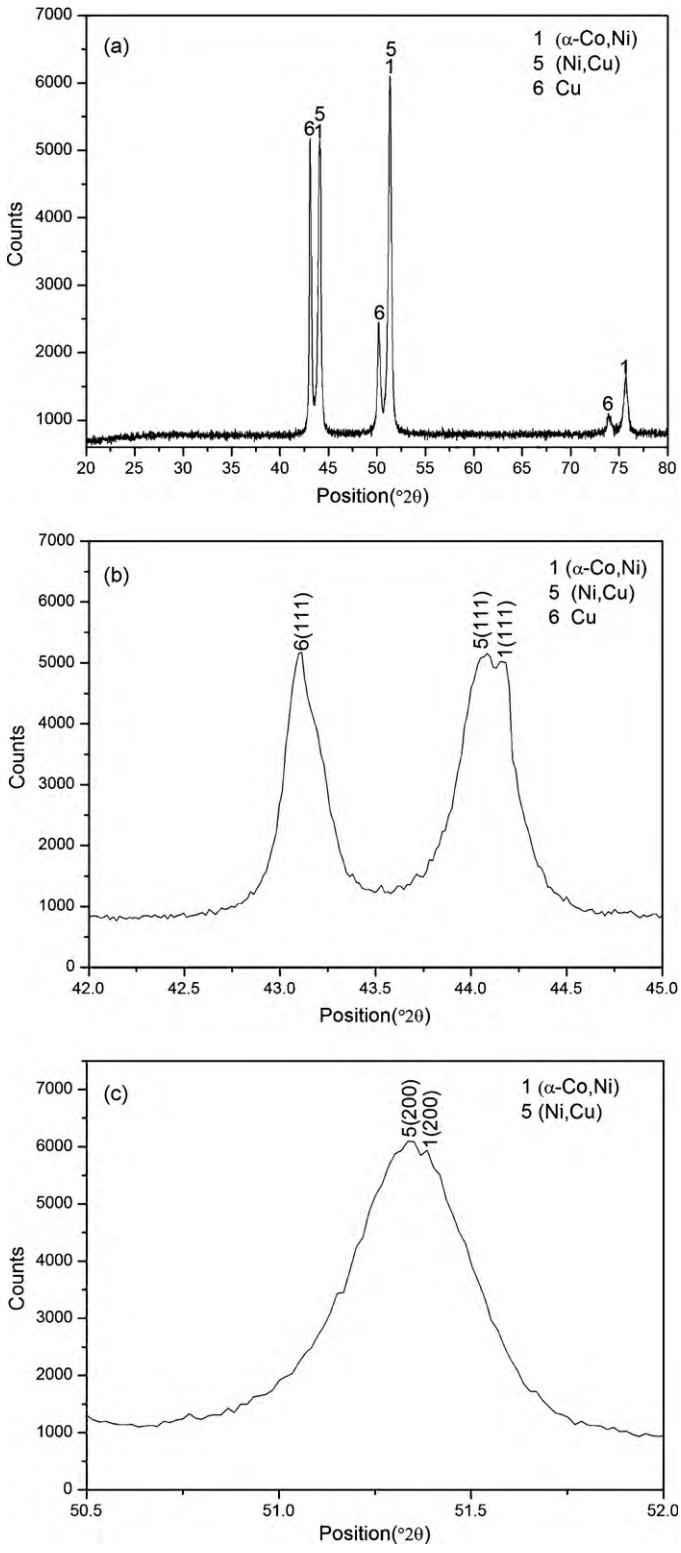

Fig. 7. XRD spectra of interfacial area: (a) 20–80°, (b) 42–45° showing the details, and (c) 50.5–52° for details.

This means that Ni has been alloyed into copper substrate.

TEM micrographs and their corresponding selected area electron diffraction (SAED) patterns of the cobalt-based coating are shown in Fig. 10, which exhibit the existence of Co-based solid solution and $Cr_{23}C_6$ hard phases, in agreement with the XRD results. TEM observation revealed the presence of $C_{23}C_6$ along the grain boundary of the α-Co (Fig. 10b). $C_{23}C_6$ is metal rich carbide, which possesses a complex cubic structure, containing 92 metal and 24 carbon atoms per unit cell, with a lattice parameter of about 1.06 nm.

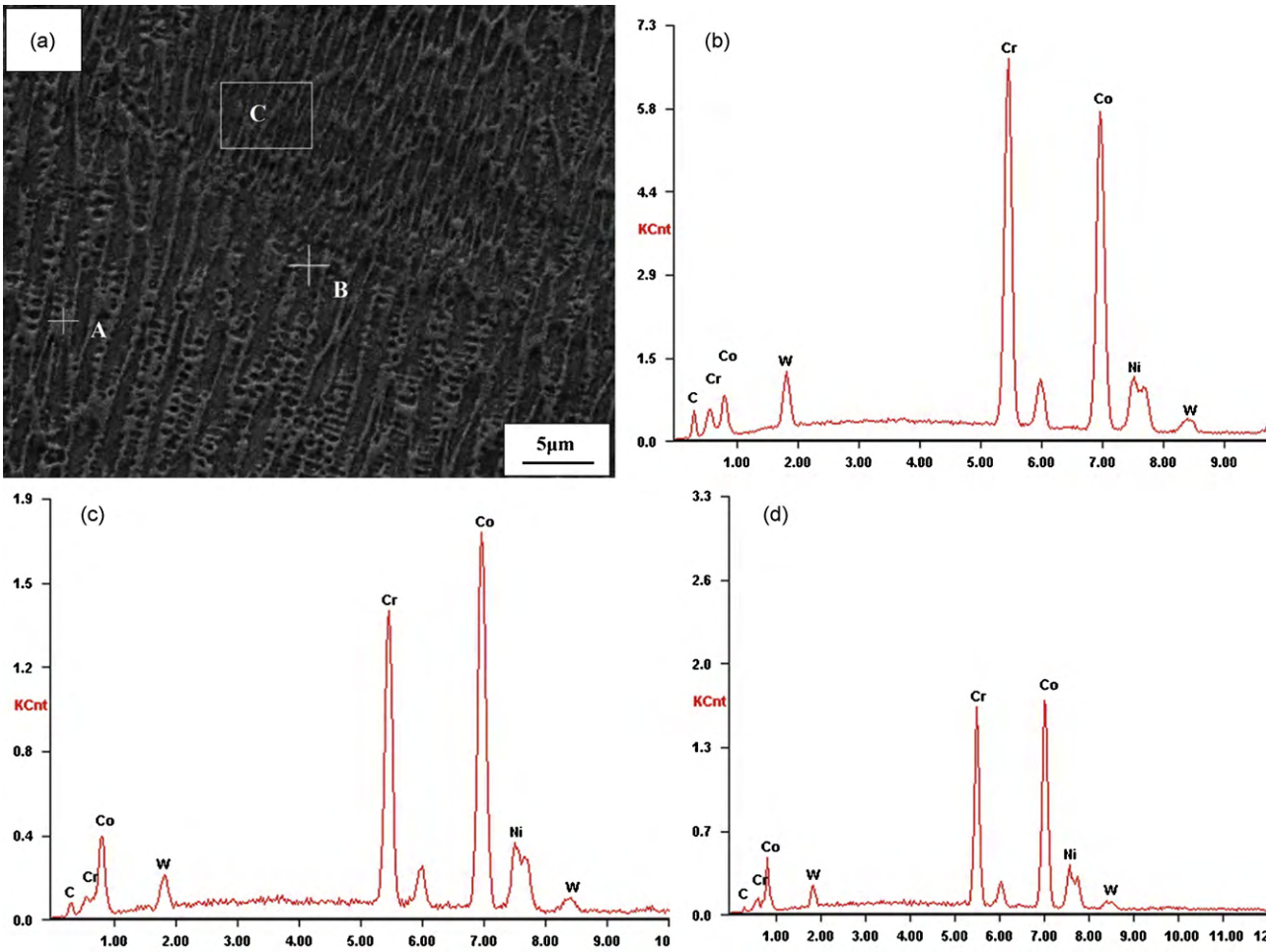

Fig. 8. SEM morphology and EDX spectra of LSC coating: (a) SEM morphology, (b) spectrum of point A, (c) spectrum of point B and (d) spectrum of rectangle C.

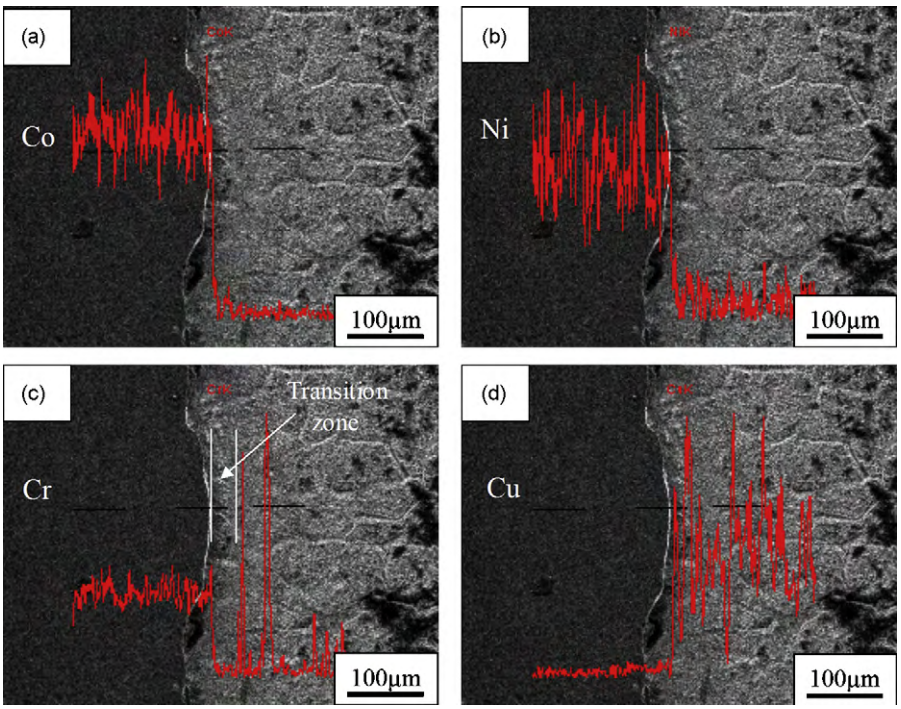

Fig. 9. SEM micrograph of the cladding/substrate region and corresponding Co, Ni, Cr and Cu EDX line-scans (acquired along the indicated line, in arbitrary units).

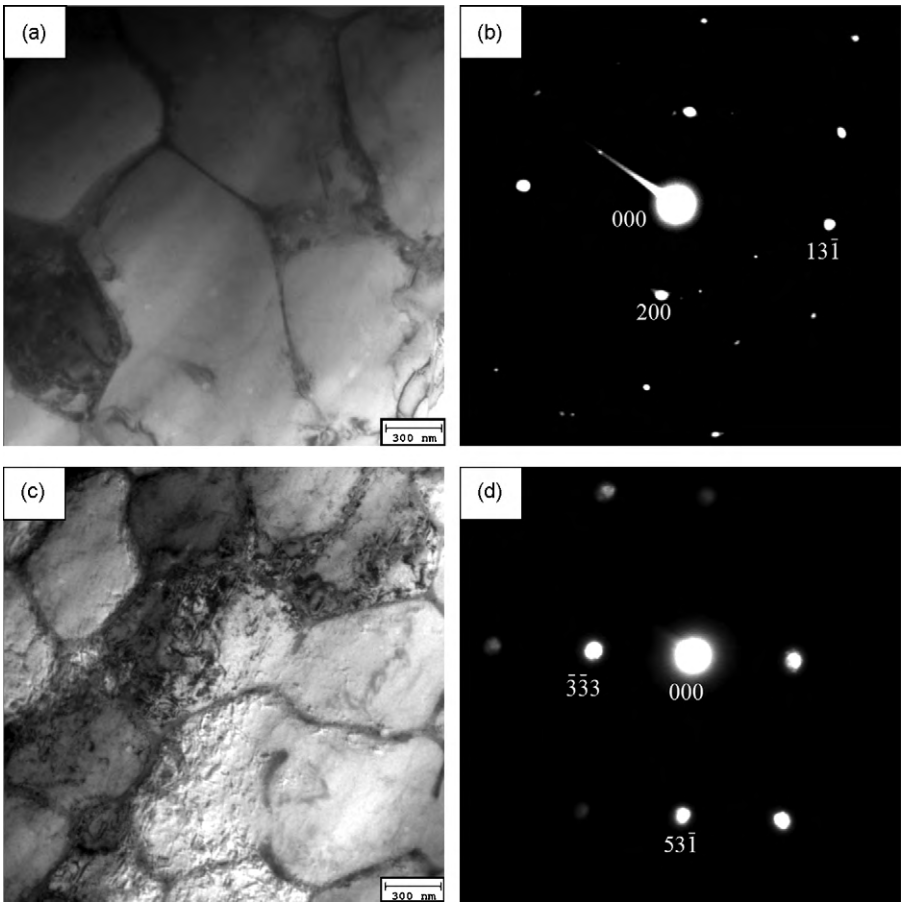

Fig. 10. TEM bright-field micrographs and their corresponding SAED patterns of LSC coating: (a) α-Co and (b) $Cr_{23}C_6$.

3.3. Microhardness and wear resistance

Variation of microhardness along the depth of LSC Co-based coating is charted in Fig. 11. Clearly, the hardness on the LSC coating was even. Average hardness value about 478 $HV_{0.1}$ of the multilayer coating was obtained, almost 5 times that of the copper substrate (92 $HV_{0.1}$). This is because carbide and intermetallics hard phases were formed during LSC. Furthermore, the hardness of Co-based coating is higher than the reported hardness 347 HV of laser post-treat the plasma-sprayed coatings by Nd:YAG [22].

As a rule, the relative wear resistance is employed to evaluate the wear performance of materials. In this study, the wear rate of copper was assumed to be a criterion, and the wear resistance of Co-based coating was defined as reciprocal ratio of copper's wear rate under the same dry sliding wear conditions. Fig. 12 gives the relative wear resistance of LSC Co-based alloy. It shows that the relative wear resistance of LSC Co-based alloy coating is more than 15,

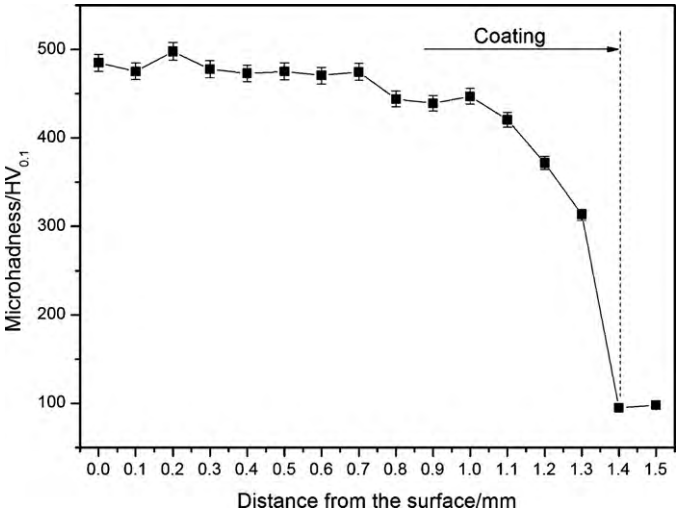

Fig. 11. Variation of microhardness along the depth of LSC specimen.

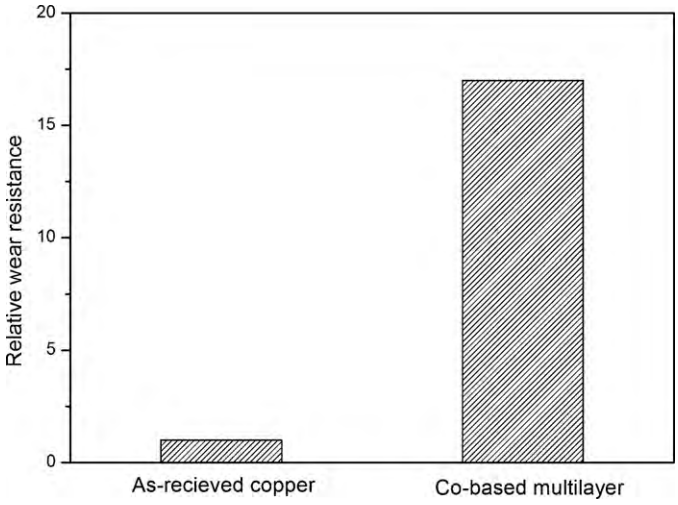

Fig. 12. Wear resistance of LSC Co-based alloy coating and as-received copper.

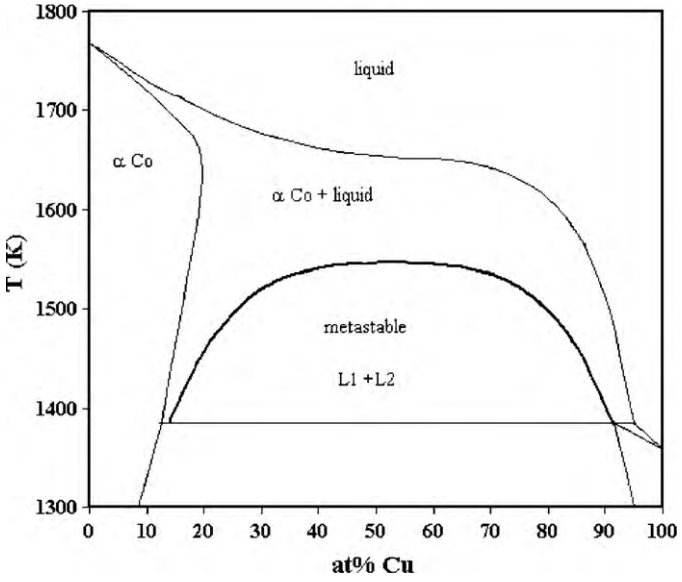

Fig. 13. Binary phase diagram of Cu–Co.

which indicates that wear resistance of copper can be significantly improved.

4. Discussion

Though LSC improves the surface performance of many materials, the reports on how to obtain thick coatings are limited. The reason is that copper possesses high reflectivity to laser, poor wettability with many materials as well as high coefficients of thermal expansion ($17 \times 10^{-6}\,^{\circ}C^{-1}$). The wave length of Nd:YAG laser (1.06 μm) is just about one-tenth of that of CO_2 laser (10.06 μm), which endows Nd:YAG laser high coupling efficiency with some metals. Based on this, direct LSC Co-based multilayer coating on copper substrate was carried out by an Nd:YAG laser using powder bed in this study. The absorbance of powder bed to laser energy is higher than its solid bulk material while its thermal conductivity is much lower than that of the solid bulk because of porous structure. This is very critical for preparing coatings on copper surface because of excellent thermal conductivity of copper.

During laser processing, two different composition zones existed inside the molten pool at the early stage: the Co-based alloy melt zone and the Cu melt zone. The intensive thermal effect often sufficiently causes efficient solute redistributions and thus generates the homogeneous distribution of elements. As the powder bed melted, the Cu absorbed most energy and was heated to a high temperature. At this stage, the Co-alloy was dissolved into the Cu melt. The molten pool is stirred with the thermal and convection effect, resulting in the homogeneous distribution too. LSC is a nonequilibrium solidification process, which forms three typical microstructures (i.e. planar, columnar and dendritic). High G/R (G is temperature gradient and R is solidification speed of crystal) is the driving force of the planar crystallization formation, due to the heat diffused downward and cooling from the environment. The molted Co-based powder and partially molten copper were bonded by diffusion and mixture forming a planar crystallization region (as shown in Fig. 5c). The columnar region is close to the planar crystallization region. The G is decreased in rising edge of the planar crystallization region and the crystallization rate is continuing to speed up, which results in interface perturbation and forms columnar. Dendrites are formed in the rising edge of the planar crystallization region or columnar region. LSC involves a complex process of the solute redistribution. The solute of high concentration liquids is easy to concentrate and the unusual composition undercooling is the main reason for the formation of dendritic microstructure. Heat is discretionarily conducted apart from the molten pool and the shape of molten pool is irregular, which makes

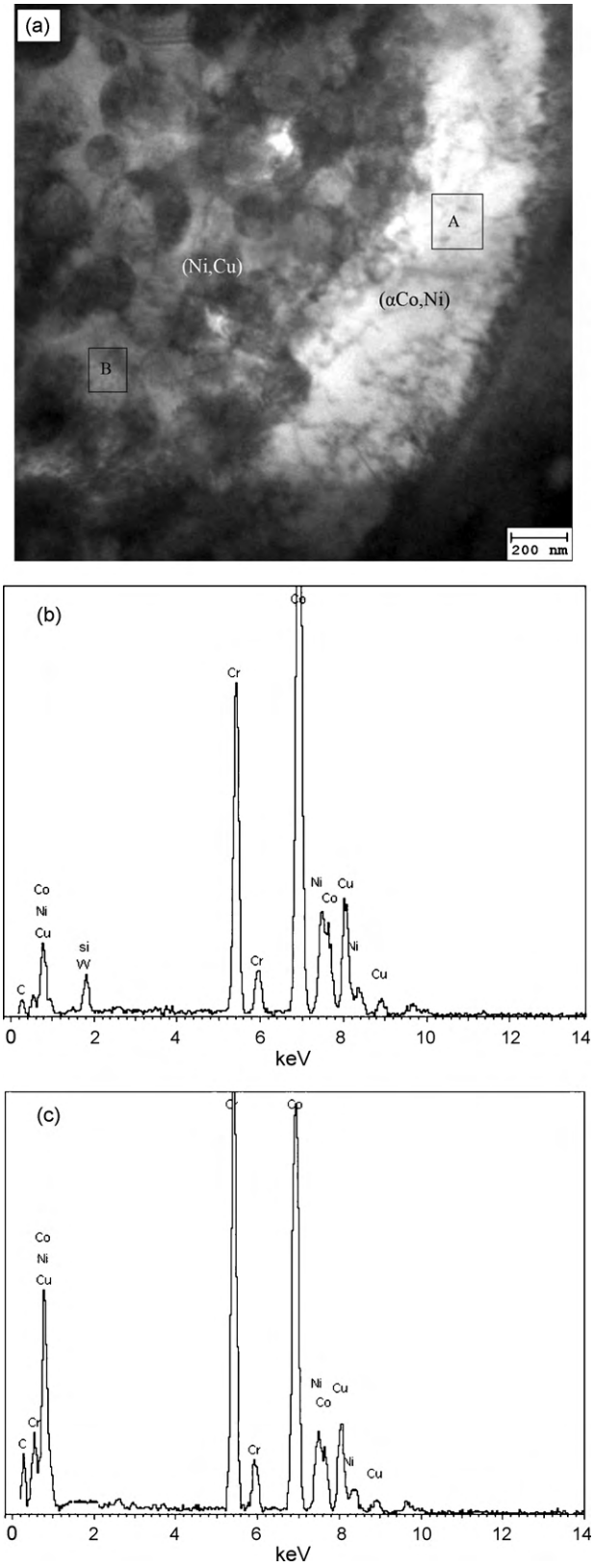

Fig. 14. TEM image of the interfacial zone of LSC specimen (a), EDX spectrum of rectangle A in white area (b) and rectangle B in grey area (c).

Table 3
Elemental atomic concentration for TEM image in Fig. 14(a) by EDX analyses.

Spectrum	Chemical composition (wt.%)						
	C	Si	Co	Ni	Cu	W	Cr
White image	1.12	1.26	48.79	14.21	9.44	1.97	22.21
Gray image	1.10	–	11.88	14.32	48.51	–	23.19

the growth orientation of dendrites different (see Fig. 5c). The solidification rate at upper region of molten pool is higher than that in the middle, therefore, second dendritic arm spacing is decreased (see Fig. 5a and b).

According to the XRD results (Fig. 6), phase structure of the Co-based coating was mainly comprised of α-Co, $Cr_{23}C_6$ and some $Ni_{17}W_3$, $Cr_4Ni_{15}W$. $Cr_{23}C_6$ and α-Co were formed during the rapid solidification of molten pool. A small amount of Cr, Ni and W was dissolved into α-Co and $Cr_{23}C_6$ (Fig. 8), which generated metastable phases possessing face-centered cubic (fcc) structures or complicated centered structure. As shown in Fig. 6, only diffracted intensity of α-Co is higher, which is caused by the preferred orientation of crystal growth during solidification by LSC. $Ni_{17}W_3$ and $Cr_4Ni_{15}W$ were formed due to the nonequilibrium solidification by LSC. The results were different from the literature [21]. It was reported that β-Co and Co_3Mo_2Si were formed in Triballoy 66FNS coating by CO_2 laser cladding.

Co and Cu are usually difficult to directly combine under equilibrium condition. However, it was interesting that perfect interface was obtained via LSC in this experiment. The binary diagram of Co and Cu exhibits a metastable miscibility gap in the metastable phase diagram [23,24], as shown in Fig. 13. In contrast to systems with a stable miscibility gap, the demixed microstructure can be access by rapid solidification [25]. That's to say, pure Co can hardly be metallurgically combined with pure Cu. But Ni and Cu has complete miscibility with each other, which forms an ultimate mutual solution, and there is good miscibility between Co and Ni, which exhibits complete solid solubility in the (α-Co, Ni) phase at temperatures between the solidus and the solvus of the α(fcc) ↔ (hcp) transformation temperature. The Bright-field TEM image of the interfacial zone of the specimen is demonstrated in Fig. 14. EDX analyses of rectangle A in white area and rectangle B in grey area depict that white phase is Co-rich and grey phase is rich in Cu and Cr (see Fig. 14b, c and Table 3). Based on XRD analysis of interface zone (Fig. 7), TEM image (Fig. 14a) and EDX analyses (Fig. 14b, c and Table 3), it was indicated that the white image was the (α-Co, Ni) and the gray zone was (Ni, Cu). It was identical with EDX line analyses of across the interface between coating and copper substrate (Fig. 9). The contents of Ni and Cu had minor fluctuations in interface region. In other words, the presence of Ni in as-received powder concatenated the Co and Cu, which generated metallurgical bonding by diffusion in the interface between Co-based coating and copper substrate.

5. Conclusions

With preplacement powder to improve the absorptivity of copper substrate to laser energy, Co-based alloy multilayer coatings were successfully fabricated with laser power of 360 W and scanning speed of 5 mm s^{-1} by a pulsed Nd:YAG laser system. The large-area coatings with a thickness of 1.5 mm were free of defect with excellent metallurgical bonding to copper substrate.

The microstructures of LSC Co-based coating were mainly composed of dendrites, cellular and planar. XRD analyses indicated that the phases of α-Co solution, $Cr_{23}C_6$, $Ni_{17}W_3$ and $Cr_4Ni_{15}W$ were formed in the Co-based coating, while (α-Co, Ni) and (Ni, Cu) solid solutions were exhibited at interface.

The LSC Co-based coating was compatible to copper substrate. The hardness of the multilayer coating was about 5 times of that of the copper. The relative wear resistance of LSC Co-based alloy coating was more than 15, which indicated that wear resistance of copper could be significantly improved.

Acknowledgements

The authors thank for the Analytic and Testing Center of Huazhong University of science & Technology for their assistance. The authors also thank Ma Xiao in Purdue University (U.S.) and Xiong Zhaoting in Loughborough University (U.K.) for their assistance in English polish.

References

[1] Y.X. Gan, J. Sweetman, J.G. Lawrence, Mater. Lett. 64 (2010) 449–452.
[2] Y. Niu, X. Zheng, H. Ji, L. Qi, C. Ding, J. Chen, G. Luo, Fusion Eng. Des. (2010), doi:10.1016/j.fusengdes.2010.04.032.
[3] J.S. Kim, Y.S. Kwon, O.I. Lomovsky, D.V. Dudina, V.F. Kosarev, S.V. Klinkov, D.H. Kwon, I. Smurov, Compos. Sci. Technol. 67 (2007) 2292–2296.
[4] W.M. Song, G.R. Yang, J.J. Lu, Y. Hao, Y. Ma, Wear 262 (2007) 868–875.
[5] F. Lusquinos, R. Comesana, A. Riveiro, F. Quintero, J. Pou, Surf. Coat. Technol. 203 (2009) 1933–1940.
[6] J. del Val, R. Comesana, F. Lusquinos, M. Boutinguiza, A. Riveiro, F. Quintero, J. Pou, Surf. Coat. Technol. 204 (2010) 1957–1961.
[7] Y.J. Huang, X.Y. Zeng, Appl. Surf. Sci. 256 (2010) 5985–5992.
[8] F.J. Wang, H.D. Mao, D.W. Zhang, X.Y. Zhao, Appl. Surf. Sci. 255 (2009) 8846–8854.
[9] V. Fallah, S.F. Corbinand, A. Khajepour, Surf. Coat. Technol. 204 (2010) 2400–2409.
[10] M. Zheng, D. Fan, X.K. Li, J.B. Zhang, Q.B. Liu, J. Alloys Compd. 489 (2010) 211–214.
[11] M. Hazra, A.K. Mondal, S. Kumar, C. Blawert, N.B. Dahotre, Surf. Coat. Technol. 203 (2009) 2292–2299.
[12] Y.L. Yang, D. Zhang, W. Yan, Y.R. Zheng, Opt. Laser Eng. 48 (2010) 119–124.
[13] S.T. Zhang, J.S. Zhou, B.G. Guo, H.D. Zhou, Y.P. Pu, J.M. Chen, J. Alloys Compd. 473 (2009) 462–466.
[14] K.W. Ng, H.C. Man, F.T. Cheng, T.M. Yue, Appl. Surf. Sci. 253 (2007) 6236–6241.
[15] F. Liu, C.S. Liu, S.Y. Chen, X.Q. Tao, Y. Zhang, Opt. Laser Eng. 48 (2010) 792–799.
[16] Y.Z. Zhang, Y. Tu, M.Z. Xi, L.K. Shi, Surf. Coat. Technol. 202 (2008) 5924–5928.
[17] Y.T. Pei, V. Ocelik, J.T.M. De Hosson, Mater. Sci. Eng. A 342 (2003) 192–200.
[18] A.H. Wang, H.B. Xia, W.Y. Wang, Z.K. Bai, X.C. Zhu, C.S. Xie, Mater. Lett. 60 (2006) 850–853.
[19] D.D. Gu, W. Meiners, Y.C. Hagedorn, K. Wissenbach, R. Poprawe, J. Phys. D 43 (2010) 135402.
[20] A.H. Wang, X.L. Zhang, X.F. Zhang, X.Y. Qiao, H.G. Xu, C.S. Xie, Mater. Sci. Eng. A 475 (2008) 312–318.
[21] G. Dehm, M. Bamberger, J. Mater. Sci. 37 (2002) 5345–5353.
[22] F. Liu, C.S. Liu, S.Y. Chen, X.Q. Tao, Z.F. Xu, M. Wang, Surf. Coat. Technol. 201 (2007) 6332–6339.
[23] D.W. Zeng, C.S. Xie, M.L. Hu, A.H. Wang, W.L. Song, Surf. Coat. Technol. 200 (2006) 4065–4071.
[24] I. Egry, L. Ratke, M. Kolbe, D. Chatain, S. Curiotto, L. Battezzati, E. Johnson, N. Pryds, J. Mater. Sci. 45 (2010) 1979–1985.
[25] S. Bysakh, K. Chattopadhyay, T. Maiwald, R. Galun, B.L. Mordike, Mater. Sci. Eng. A 375–77 (2004) 661–665.